The 6th International Conference on Nuclear Thermal Hydraulics, Operations and Safety (NUTHOS-6)
Nara, Japan, October 4-8, 2004.
Paper ID. N6P007

DIRECT CONTAINMENT HEATING INVESTIGATIONS FOR EUROPEAN PRESSURIZED WATER REACTORS

L. Meyer, G. Albrecht, D. Wilhelm

Institut für Kern- und Energietechnik
Forschungszentrum Karlsruhe GmbH
Postfach 3640, 76021 Karlsruhe, Germany
meyer@iket.fzk.de

KEY WORDS

Severe accident, Vessel failure, Direct Containment Heating, Melt Dispersion

ABSTRACT

While the issue on Direct Containment Heating (DCH) was resolved for US reactor plants in the 1990s it was found that the consequences of DCH processes are strongly dependent on the reactor cavity configuration. Therefore, an experimental and analytical program was started in 1998 to investigate melt ejection scenarios for typical German and European reactor designs. Six experiments have been performed in a 1:18 scaled reactor geometry, characterized by a narrow pit without exit other than through the annular space between pressure vessel and cavity wall, leading either directly to the upper containment or into the pump and steam generator rooms along the flow path around the main cooling lines. The corium was modeled by an iron-alumina melt that was driven by steam, and a prototypic atmosphere in the containment was applied. Since the system pressure at core melt accidents will be low due to compulsory system depressurization, the vessel failure pressures were kept between 0.8 and 2.2 MPa in these experiments. The experiments showed the importance of the direct path from the reactor pit to the containment. Without that path, there will be a considerable ejection of melt into the pump and steam generator rooms, but almost nothing into the open space of the containment. The hydrogen production and combustion will also be lower. Consequently, the pressure increase will stay moderate and well below the design pressure of most containments. The experiments are analyzed by a CFD code with the objective to transform the experimental results to the reactor case.

1. INTRODUCTION

The conditions in the reactor pressure vessel (RPV) in the late phase of a core melt accident can differ significantly depending on the failure history of the core (Seghal, 2001). If a failure of the RPV lower head occurs, the condition of the molten core, i.e. temperature, composition, distribution, and mass of the melt, together with the design of the lower head, determines the location, shape and size of the breach. The decisive parameter for the mode of melt release is the system pressure at the time of RPV-failure. If the pressure is at the same level as the pressure in the containment, or only slightly above, the molten part of the core inventory will flow into the reactor pit by gravity. The release of radioactive aerosols will be small and the further development of the accident is determined by the specific plant provisions. The assumption that the system pressure at core melt accidents will be low (< 2 MPa) in German plants is justified, due to the pressure reduction system provided and the fact that a failure of the surge line is expected in such cases (Roth, 1994). However, if the pressure is between 0.5 and 2.0 MPa, e.g. because of late reflooding and rapid steam generation, the melt will be ejected forcefully into the reactor pit and possibly beyond, even at these low pressures, accompanied by the blowdown of the reactor cooling system. In this case it depends on the cavity geometry

whether the melt will be trapped without severe consequences in places with long term cooling capabilities or whether it will be dispersed into the containment atmosphere with unfavorable effects upon the accident progress. The finely fragmented melt particles lead to efficient debris-to-gas heat transfer, hydrogen generation by metal/steam reactions in the reactor pit and hydrogen combustion in the containment. These processes, referred to as Direct Containment Heating (DCH), may cause a rapid increase in temperature and pressure in the containment and may have an impact on vital safety components.

DCH is a relatively well resolved issue for reactor plants with cavity designs without a direct path to the containment, where a large instrument tunnel is connected to reactor sub-compartments. A research program devoted to high pressure melt ejection (HPME) in US-reactor designs, relating to small holes centered at the lower head, was concluded in 1998 with two important findings (Pilch,1996).

1. The main part of the corium is trapped in these intermediate rooms, and the DCH-processes have less impact due to constraints in available volume and time, thus the pressure build up in the containment stays below the design pressure.
2. The results regarding melt dispersion and DCH are extremely dependent on geometric parameters.

Thus, for Westinghouse plants consensus was reached on the adequacy of the existing containment systems to meet the challenge posed by DCH. Experiments, carried out with cavities similar to Combustion Engineering plants, that are partially open to the containment through the annular space between the vessel and the pit, have shown that a considerable amount of melt can be dispersed into the containment, and the containment pressure can increase rapidly by several bars (Blanchat, 1996 and Blanchat, 1999). For these reactor designs depressurization of the reactor cooling system below the so called DCH cut off pressure was suggested to mitigate DCH loads on the containment. The level of the cut off pressure, however, may lie below 1 MPa, depending on the breach size in the RPV. Therefore, and because failure modes other than small holes were envisaged, a research program on DCH for European reactor designs was launched in 1998.

At Forschungszentrum Karlsruhe (FZK), experiments were performed with cold model fluids in a test facility (DISCO-C) scaled 1:18 to a large PWR, to study the fluid dynamic processes with different failure modes of the bottom head under low pressure conditions ($p \leq 1.5$ MPa). The fluids employed were water or a bismuth alloy instead of corium, and nitrogen or helium instead of steam. The main results from the cold experiments were: large holes ($Ø \geq 0.5$ m, scaled) at the base of the bottom head lead to high dispersed melt fractions (> 50%). The maximum dispersed fraction for such breaches is reached already at pressures below 2.0 MPa. A certain amount is trapped in the reactor pit depending on its geometry. With breaches at the side of the lower head, the dispersed melt fraction is lower and, even with unzipping of the bottom head, the dispersed fraction is smaller than with central holes (Meyer, 2003). In a second facility (DISCO-H) selected experiments in the same scale were performed with an iron-alumina melt, steam and a prototypic atmosphere in the containment. These experiments are designed to investigate the fluid-dynamic, thermal and chemical processes during melt ejection out of a breach in the lower head of a PWR pressure vessel at pressures below 2 MPa. The results of the first six experiments performed in the DISCO-H facility are presented in this paper.

The objective of our program is to develop codes that can be applied to the safety analysis of severe accidents in light water reactors. The first step is to introduce DCH-specific models into existing multi-phase, multi-field codes and recalculate the experiments (Wilhelm, 2002 and 2003). By comparison of code results with experimental data these models are being qualified. Results from code analysis of the present six experiments are presented in this paper. Together with this work the extrapolation of the evaluation to the reactor scale and material has to be ensured. In a second step simple models or correlations will be derived from this work, and will be introduced in fast running system codes which will be used for probabilistic safety assessment studies.

2. THE EXPERIMENTAL FACILITY AND PROCEDURE

2.1 Components of the DISCO-H Facility and experimental procedure

The model of the containment pressure vessel has an outer diameter of 2.20 m and a height of 4.60 m; with the pedestal and the top port its total height is 5.80 m (Fig. 1). The lower head is filled with concrete that forms a level floor. All internal structures are bolted to that floor. At the center of the floor is a large vertical pipe that contains the condensate draining piping and has a connection to the bottom port. The entire vessel is insulated against heat loss on the outside by a 100 mm thick fiberglass insulation. The empty volume of the containment vessel is 14.18 m³, the total freeboard volume including the subcompartment is 13.75 m³. The containment model is heated over a time period of approximately 12 hours by filling with steam additional to the atmospheric air until the vessel pressure reaches 0.2 MPa. The condensate water is drained at the bottom of the vessel from time to time. The average gas temperature and the wall temperature inside the vessel is 373 K (100°C) at the end of the heat-up. A metered amount of hydrogen gas (approximately 3 mol%) is added to the vessel at the end of heat-up while fans are running inside the vessel. A gas sample is taken just before the start of the experiment.

The subcompartment is an annular space around the cavity with a volume of 1.74 m³. The flow path from the cavity into the subcompartment is along the eight stubs modeling the main cooling lines (total flow cross section is 0.0308 m²). The top cover has four openings with a diameter of 130 mm, that are covered by a wire mesh to prevent melt to enter the containment.

The RCS-RPV pressure vessel models the volumes of both the reactor cooling system (RCS) and the reactor pressure vessel (RPV) and has a total volume of 0.076 m³. A disk holding 8 pipes (46 mm I.D., 255 mm length) separates the two partial volumes. This arrangement models the main cooling lines with respect to the flow constriction between RCS and RPV. The vessel (inner diameter 0.20 m) is heated electrically, and is insulated over the whole length and on the top. It is heated to the saturation temperature of the planned burst pressure, e.g. to 453 K (180°C at 1.0 MPa). It contains nitrogen at that temperature at 0.1 MPa (Fig.2).

The steam accumulator is a cylindrical pressure vessel placed outside of the containment pressure vessel with approximately the same volume (0.082 m³) as the RCS-RPV pressure vessel. Both vessels are connected by a 25 mm diameter pipe with an electro-pneumatically actuated valve. The steam accumulator is heated electrically to the saturation temperature of twice the planned burst pressure, e.g. 486 K (213°C at 2.0 MPa). It is filled with a measured amount of water by a high pressure metering pump to reach that pressure.

The RPV model, that serves as crucible for the generation of the melt, is bolted to a plate carrying the RCS-RPV pressure vessel (Fig.2). An insulation material of magnesium oxide is filled between the outer shell of the RPV model and an inner steel liner, that contains the thermite powder. The hole at the bottom of the melt generator is formed by a graphite annulus. It is closed with a brass plate. The hole diameter was 56 mm or 28 mm (100 cm or 50 cm scaled) in the present experiments. The RPV model is filled with aluminum-iron-oxide thermite. The experiment is started by igniting the thermite electro-chemically at the upper surface of the compacted thermite powder. When a pressure increase in the RPV-RCS pressure vessel verifies that the thermite reaction has started, the valve in the line connected to the accumulator is opened and steam enters the pressure vessel. The valve is closed again after two seconds, by that time the pressure in the RPV-RCS vessel and the accumulator has equilibrated. The amount of steam that is initially in the RCS-RPV pressure vessel is determined by the amount of water originally in the accumulator minus the water left in the accumulator. The steam flow takes approximately one second. During that time and thereafter the thermite reaction progresses until it reaches the bottom of the RPV vessel. 3 to 8 seconds after ignition the brass plug at the bottom of the RPV vessel is melted by the 2400 K hot iron-alumina mixture. That initiates the melt ejection.

By that time the pressure in the RCS-RPV pressure vessel will be higher than the preset value due to radiation heat transfer from the hot melt to the steam. The melt is driven out of the breach by the steam and is dispersed into the cavity and the containment. Due to the melt-to-gas heat transfer, exothermic metal/oxygen reactions, and hydrogen combustion the pressure and temperature in the containment pressure vessel will rise. 10 seconds after blow-down, the fans, which had been shut down before the start of the test, are started again, and at 20 or 30 seconds the post test gas samples are taken.

The reactor pit is made of concrete (Fig. 2) and is installed inside a strong steel cylinder (30 mm thick walls). Besides the flow path along the main cooling lines into the subcompartment, there is the option of a flow out of the cavity straight up into the containment through eight openings with a total cross section of 0.052 m².

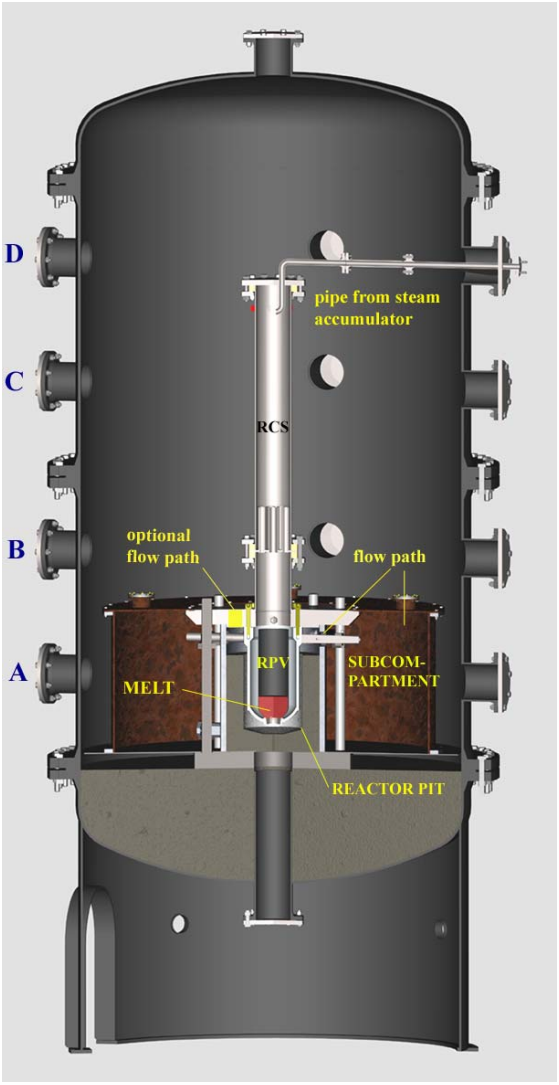

Fig. 1. Scheme of the test facility

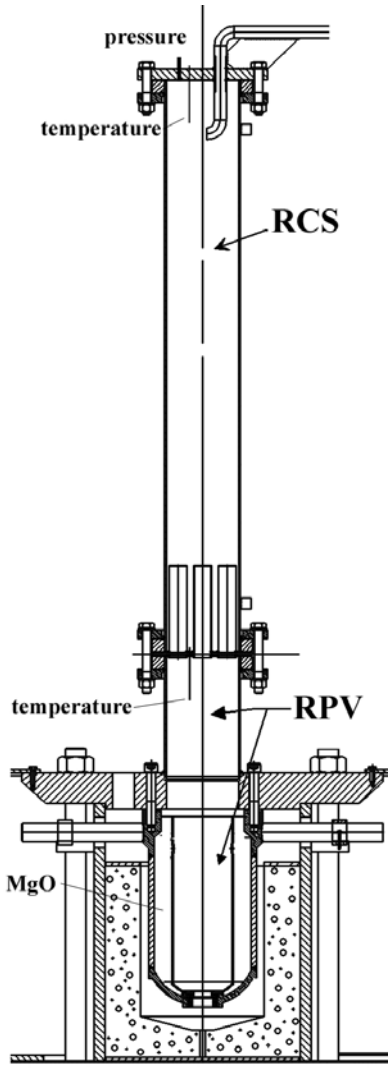

Fig.2. The RPV-RCS model and reactor pit

2.2 Instrumentation

Standard test results are: pressure and temperature history in the RPV, the cavity, the reactor compartment and the containment, post test melt fractions in all locations with size distribution of the debris, video film in reactor compartment and containment (timing of melt flow and hydrogen burning), and pre- and post test gas analysis in the cavity and the containment.

Generally, type-K thermocouples are installed in the facility. They are steel sheathed thermocouples with insulated wires. The outer diameter of the sheath is 0.35 mm. The steam temperature in the accumulator tank is measured by two thermocouples, one near the top and one near the bottom. There are two thermocouples within the RCS-RPV pressure vessel, one in each compartment (RCS and RPV). A total of 11 thermocouples are located at different levels in the containment pressure vessel to measure the bulk gas temperature. Two of them are within the subcompartment, one is at the floor and the rest is either close to the wall or in the space between the RCS-RPV pressure vessel and the containment wall.

A total of 15 strain gauge-type pressure transducers (Kulite) with ranges of 0–1.7 MPa, 0–3.4 MPa and 0–7.0 MPa are used to measure steam and gas pressures. The compensated operating temperature range is 27°C – 232°C, with a thermal drift of +/- 5% of full scale output. The transducers are adjusted at the operating temperature just before the start of the experiment.

Ten pre-evacuated 500-cm³ gas grab sample bottles are used to collect dry-basis gas samples at three positions, in the cavity, in the subcompartment, and in the upper part of the containment. The sample lines and the sample bottles are cold, thus the bottles are filled with non-condensable gases only. One pretest sample collects background information just prior to the start of the melt ejection. One sample at all three stations is taken during the blow down and one 20 seconds after the blow down.

Three video cameras are used in the experiment. One camera looks down from the dome into the containment, one is installed at the level B port looking at the top of the subcompartment and the openings in the top plate, that represent the direct path from the cavity into the containment. A third camera looks into the compartment from level A port by means of an endoscope.

The total debris mass dispersed into the DISCO vessel and the debris mass in specific locations is determined by a posttest debris recovery procedure. A posttest sieve analysis of the debris recovered from different locations is performed for each test.

In a scoping tests, the melt plug was filmed by a high speed camera (500 frames/s) from below and the side. From these pictures we can infer, that the melt plug is fully open within 2 ms. Posttest inspection of the melt plug exit area determined that the exit hole was round, fully open, and with a diameter of about 55 mm. A 0.5 mm thick film of melt coated the carbon ring that formed the exit hole. A thin film of melt also coated most of the interior steel liner of the crucible. Some of the steel liner had melted exposing the MgO insulator, particularly at the bottom of the liner.

2.3. Scaling considerations

The geometrical linear scale is 1:18, thus volumes of gas and liquid are scaled accordingly (length scale to the power of 3). The initial pressure can be scaled 1:1, and the duration of the blowdown is scaled as the length scale. Then, the gas velocity and the droplet size are mainly functions of the properties of the model fluids used. Table 1 shows the composition of the used melt. Before ejection, the melt separates into the two main components, iron on the bottom and alumina on top. The maximum potential hydrogen produced by the reaction with steam is 101 moles with iron and 6 moles with aluminum. The properties of the melt mixture are listed in Table 2 together with those of a typical corium mixture (Blanchat, 1999). Important for the similarity of the thermal and chemical processes is the energy content of the melt. The combined thermal and chemical energy is 1.47 MJ/kg for corium and 2.83 MJ/kg for the model melt. Thus the scaling of melt mass is difficult. The scaled up mass of 10.6 kg melt gives 62000 kg, which has a volume of 16 m^3 and a combined energy of 175000 MJ. The volume of 16 m^3 corium would have a mass of 128000 kg and a total energy of 188000 MJ. Thus, the volume and energy content is scaled relatively correct, while the mass scaling is off by a factor of 2.

Table 1. Composition of melt in DISCO-H

	Mass Fraction	Mole Fraction	Volume Fraction
Fe	0.53	0.66	0.33
Al	0.01	0.03	0.02
Al_2O_3	0.46	0.31	0.65

Table 2. Material properties of melt

Property			**Corium**	**Simulant melt**
Effective molecular weight	MW_{eff}	*kg/mole*	0.2247	0.0691
Specific heat of reaction	$\Delta e_{reaction}$	*MJ/mole*	0.0371	0.0160
Specific thermal energy	$\Delta e_{thermal}$	*MJ/mole*	0.2980	0.1820
Specific combined energy	$\Delta e_{combined}$	*MJ/mole*	0.3350	0.1980
Specific heat	C_p	*J/mole/K*	119.1	82.8
Specific heat	c_p	*J/kg/K*	525.7	1198.4
Thermal conductivity	k	*W/m/K*	5.0	19.7
Density	ρ	kg/m^3	8045	3878
Kinematic Viscosity	$\nu = \mu/\rho$	m^2/s	1.88×10^{-6}	1.88×10^{-6}
Surface tension	σ	*N/m*	0.973	0.932
Melting point of oxide	$T_{mp,oxide}$	*K*	2450	2200
Temperature of melt	T_{melt}	*K*	2800	2400

3. EXPERIMENTAL RESULTS AND DISCUSSION

3.1 Test Matrix: Variations to the base case

Four parameters were varied in a systematic way in six experiments:

1. Pressure at melt plug failure
2. Flow path out of the reactor pit (w. / w.o. direct path into the containment dome)
3. Driving gas and containment atmosphere (steam/nitrogen and w./w.o. steam in the containment)
4. Hole size in RPV bottom (56 or 28 mm)

The experiment named H02 can be considered to be the base case. This experiment was performed with an open direct path from the reactor pit to the containment, with prototypical conditions concerning the steam driven ejection out of the RPV, and a containment atmosphere, that was part air and part steam at an elevated pressure, with 3 mole-% hydrogen. Test H01 had less steam in the RCS/RPV vessel, the pressure at failure was only 0.8 MPa, versus 1.2 MPa for the base case. In test H03 the direct path to the containment dome was closed, but the thermodynamic conditions were the same as in H02. In these tests, hydrogen production and combustion occurred. In the experiment H04 the hydrogen effect was excluded by using only nitrogen as driving gas and a pure air atmosphere in the containment. The only chemical reaction is the oxidation of iron in the containment atmosphere. The conditions of this experiment may not be prototypical, but it is important to separate the thermal effects from the chemical effects, to validate the respective models. Tests H05 and H06 were both performed with a smaller hole, 28 mm instead of 56 mm. Additionally, in H05 the direct path to the containment was closed again, while in H06, with an open path, the pressure at failure was raised to 2.2 MPa by filling more steam into the RCS/RPV vessel. A quick reference is given in Table 3; the exact initial conditions and the main results are listed in Table 4.

Table 3. Test matrix

	Base case ***H02***	**H01**	**H03**	**H04**	**H05**	**H06**
Pressure	***1.2***	**0.8**	1.2	0.9	1.2	**2.2**
Cavity	***open***	open	**closed**	open	**closed**	open
Driving gas	***steam***	steam	steam	**nitrogen**	steam	steam
Hole size	***56 mm***	56	56	56	**28 mm**	**28 mm**

Table 4. Initial conditions and main results

			H01	**H02**	**H03**	**H04**	**H05**	**H06**
Flow path to containment vessel			open	open	closed	open	closed	open
RPV pressure at failure		MPa	0.77	1.22	1.25	0.89	1.21	2.16
Gas composition in RPV	steam	mole	7.0	15.0	16.0	0	20.7	34.9
	N2		2.0	2.0	2.0	12.0	2.0	3.2
Containment vessel initial pressure		MPa	0.201	0.206	0.201	0.100	0.200	0.210
Containment vessel initial temperature		°C	101	102	101	17	101	103
Max. containment vessel pressure		MPa	0.370	0.442	0.315	0.256	0.290	0.404
Max. containment vessel pressure increase		MPa	0.170	0.236	0.114	0.156	0.090	0.194
Time of peak pressure		s	1.75	1.75	1.2	1.75	1.75	1.75
Pressure at time = 10 s		MPa	0.294	0.325	0.260	0.185	0.258	0.329
Max. average vessel temperature (approx.)		°C	360	530	300	450	225	450
Hydrogen in containment vessel and subcompartment	pretest	mole	-	26	27	0	29	35
	produced		-	54	33	0	32	39
	burned		-	66	35	0	26	49
Fraction of available hydrogen that burned			-	0.83	0.53	-	0.43	0.66
Duration of hydrogen combustion		s	3	6	2	0		2
Melt transport fractions	dispersed from cavity		0.355	0.605	0.458	0.753	0.377	0.486
	transported to containment		0.237	0.503	0.022	0.663	0.018	0.361
	transported to subcompart.		0.120	0.102	0.435	0.090	0.359	0.125

Table 5. Characteristics of the blow down process

No.	**d (mm)**	**Δp (Mpa)**	**u_{liquid} (m/s)**	**t_L (s)**	**t_{2ph} (s)**	**t_{end} (s)**	**t_s (s)**	**t_s/t_L -**
H01	0,056	0,580	17,3	0,050	0,240	0,470	0,107	1,34
H02	0,056	1,020	22,9	0,090	0,270	0,490	0,080	0,67
H03	0,056	1,050	23,3	0,135	0,350	0,560	0,079	0,44
H04	0,056	0,790	20,2	0,145	0,350	0,550	0,091	0,47
H05	0,028	1,010	22,8	0,260	0,580	1,600	0,323	0,93
H06	0,028	1,950	31,7	0,250	0,600	1,600	0,232	0,70

3.2 Pressure and Temperature Data

Figure 3 shows samples of the blow-down pressure and the pressures in the cavity and containment. The blow-down ends when the RPV-pressure curve meets the rising cavity pressure. It lasts approximately 0.5 seconds in the four tests H01 through H04 with the 56-mm-hole, and 1.6 seconds for tests H05 and H06, with the 28-mm-hole. Three distinct stages can be recognized in the curves of the RPV pressure: first, a slow decrease, second, a steep drop up to a maximum slope, and third a slowing down of the pressure drop. These stages can be detected better if the pressure gradient dp/dt is plotted versus time, as shown in Fig.4. An almost constant low gradient exists for a certain time at the beginning of the blow-down, which can be interpreted as a liquid single-phase or nearly single-phase jet (t_L). The second stage is a two-phase flow, starting slowly and reaching a peak volume flow when the single-phase steam flow begins (t_{2ph}). At this point of time the pressure ratio of the vessel pressure and cavity pressure is still supercritical, and choked flow prevails. In Table 5 the times of these three flow stages are listed. Also given is the theoretical velocity of the liquid jet determined by the driving pressure difference Δp and the density of the melt, ρ_M,

$$u_L = (2\,\Delta p/\rho_M)^{1/2}, \tag{1}$$

and the duration of the melt ejection, provided that all melt is ejected single-phase,

$$t_s = V_M/(\varepsilon\,\pi\,d^2/4\,u_L) \tag{2}$$

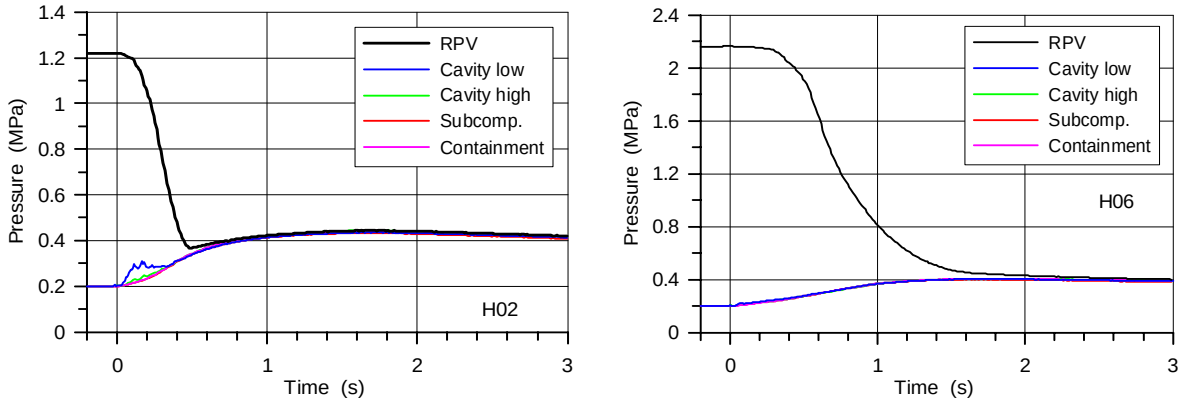

Fig. 3. Pressure in the RPV, cavity, subcompartment and containment

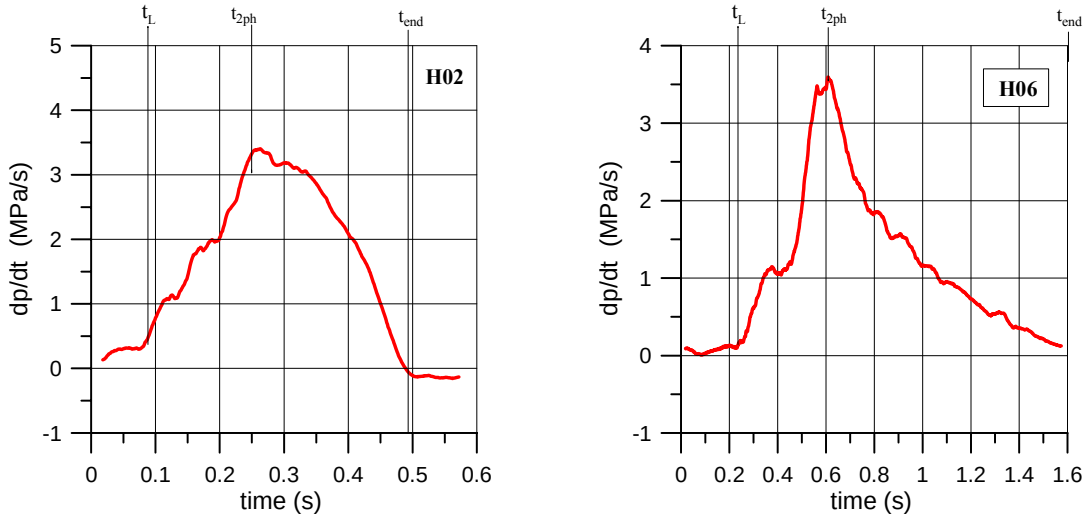

Fig. 4. Pressure gradient of the blow down pressure

with V_M, the volume of the melt, ε, the contraction factor and d, the hole diameter. However, the two components of the melt probably have separated, with the iron (ρ=6.35 g/cm^3) at the bottom and the alumina (ρ=2.8 g/cm^3) on top. Therefore, the iron will be ejected first and the alumina second. The total ejection time does not change significantly whether the well mixed melt or the separated components are ejected. The ejection time was calculated with ε= 0.8. But regardless of the chosen value, 0.5 or 0.9, the resulting times t_s are shorter than those taken from the measured data (t_{bl}), with the exception of test H01. The only plausible explanation is a larger liquid volume due to gas that was previously dissolved in the thermite melt. By contrast, in the experiments with cold water or Wood´s metal as model fluids, the theoretical time was longer than the measured time of single-phase liquid flow (Mey03). This was attributed to the gas blow-through which occurs at a certain liquid height before all liquid is blown out. Because of the large and variable divergence between theoretical and measured liquid discharge times, all models based on these theoretical data should be used with care.

During the ejection of the melt the pressure in the cavity is generally higher, by a maximum of 0.1 MPa, than in the other locations, especially in tests H02, H03 and H04. This hints to a rapid heating of the cavity atmosphere and a flow obstruction by the narrow annular cross section around the RPV. In tests H05 and H06 the melt flow is too small to cause a substantial overpressure in the cavity. Shortly after the end of the single-phase melt ejection the pressure in all locations changes uniformly.

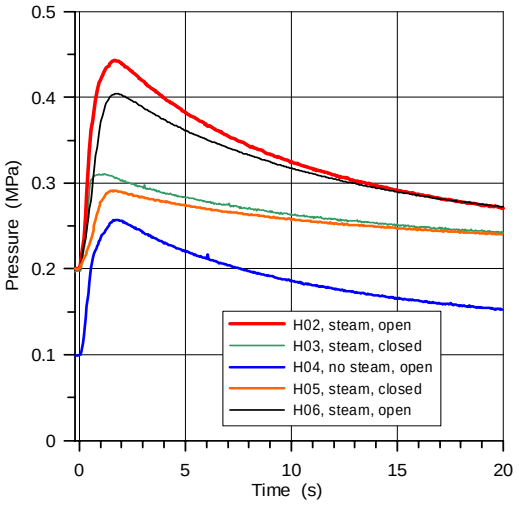

Fig.5. Long term pressure histories in the containment

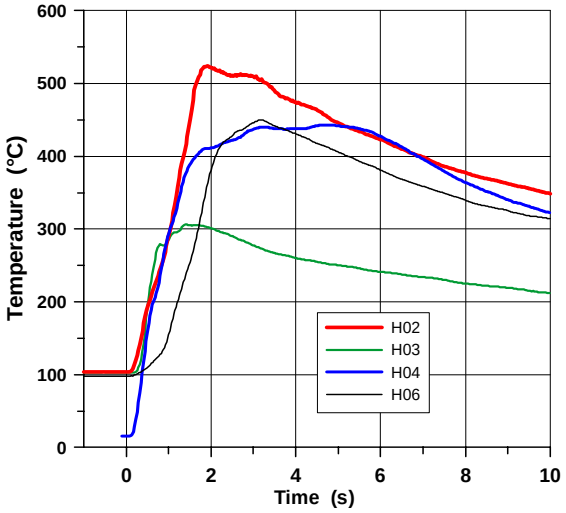

Fig.6. Average temperatures in the containment

The maximum pressure is reached between t = 1.2 and 1.75 s. Due to heat losses to the vessel walls the pressure decreases again. After approximately 10 s the pressure increase has dropped to half of its maximum value (Fig. 5).

The pressure rise in the containment is highest with an open pit and hydrogen combustion (Fig. 5). With a closed pit the gas and the debris has to flow first into the subcompartment and then through relatively small cross sections into the containment. Less hydrogen was produced and burned in this case (see Table 4). In test H04, without steam, no hydrogen effect was present, but, with the direct path to the containment open, a large amount of debris was dispersed into the containment, and efficiently transferred heat to its atmosphere. The smaller breach in tests H05 and H06 leads to a longer blow down, but to a smaller pressure rise, due to less melt dispersion out of the cavity.

The gas temperatures in the containment correspond to the pressure rises (Fig.6). It is, however, difficult to determine a representative temperature in the containment vessel, especially during the

first 4 to 10 seconds. Some thermocouples in the compartment and in the lower part of the containment registered very high gas temperatures. The temperature in the compartment is high (>800°C), because of the heat transfer from the high load of melt particles to the gas inside the small space of the compartment. Other thermocouples are close to the compartment exit holes and are within or near the hydrogen flame, that could be observed in some tests. Thus, the average was determined by those data, that were not extreme. Those from positions where the flame was burning or near the floor were not considered. Of course, this choice introduces a large uncertainty into the average temperature data.

3.3 Gas Analyses

The objective of the gas composition measurements and gas analysis is to obtain data on the chemical reactions taking place during the blow-down, that is, the production of hydrogen by the metal/steam reaction and the hydrogen combustion. We cannot distinguish these processes from direct metal/oxygen reactions, but in terms of total energy release, it makes little difference that direct metal/oxygen reaction initially deposits more energy in the debris and less in the gas, because, for small particles that react efficiently, heat transfer is also efficient.

The composition of the gas in the vessel was measured in four tests, H02, H03, H05 and H06. The gas samples were taken from an atmosphere containing a mixture of steam and noncondensible gases. The pretest composition of the vessel atmosphere is known and the amount of each gas in moles can be calculated with the volume of the vessel V, the atmosphere pressure p_0 and temperature T_0, and the measured amount of added hydrogen.

The amount of hydrogen, that is produced and burned during the test, can be determined by the nitrogen ratio method (Blanchat et al. 1994). The data and assumptions required for this method are listed below:

1. The total pretest moles of noncondensible gases must be known.
2. The measured ratios of the pretest and posttest noncondensible gases must be known.
3. It must be assumed that nitrogen is neither produced nor consumed by chemical reactions.

With the measured data of the pretest mole fractions of species i, X^0_i, the initial number of gas moles N^0_i is:

$$N^0_i = X^0_i \, (N^0_{air} + N^0_{H2} + N_{N2\ RCS/RPV}) \tag{3}$$

With the assumption that the number of nitrogen moles has not changed, the post test number of moles of oxygen and hydrogen can be determined from the measured post test mole fractions X^2_i:

$$N^2_{O2} = N^0_{N2} \, X^2_{O2} / X^2_{N2} \tag{4}$$

$$N^2_{H2} = N^0_{N2} \, X^2_{H2} / X^2_{N2} \tag{5}$$

The number of moles of burned hydrogen is linked to the decrease of oxygen moles,

$$N^2_{H2\ burned} = 2 \, (N^0_{O2} - N^2_{O2}) \tag{6}$$

and the balance of hydrogen gives the moles of produced hydrogen:

$$N^2_{H2\ produced} = N^2_{H2} - N^0_{H2} + N^2_{H2\ burned}. \tag{7}$$

The fraction burned is

$$F_{H2} = N^2_{H2\ burned} / (N^0_{H2} + N^2_{H2\ produced}). \tag{8}$$

The results show that more hydrogen is produced and burned if a direct path to the containment dome exists and if the breach is large (Table 4). The pressure rise in the containment is correlated to

the amount of burned hydrogen. Not all metal in the melt was oxidized, or in other terms, more hydrogen could have been produced with the existing metal. The ratio of hydrogen moles produced to iron moles oxidized depends on the kind of iron oxide formed. Based on the experience at the Sandia National Laboratories, Blanchat et al. (1999) gives a ratio of 1:1, which implies that in a first step only FeO is formed. For aluminum it is 1.5:1, 3 moles of hydrogen are produced by the oxidation of 2 moles of aluminum with water. The potential maximum hydrogen production would be 101 moles by iron and 6 moles by aluminum, more than actually found in the experiments.

3.4 Video observation results

Pictures taken from the top port during test H06 are shown in figure 7 as an example. The dark round object at the center is the top of the RCS-vessel. The cavity exit openings, which are 2 meters below, can be seen in the first picture. Up to t = 840 ms melt particles are airborne. Between t = 1160 ms and t = 1240 ms a bright orange glow hints to a hydrogen flame.

Fig. 7. Downward view from top port during test H06

3.5 Debris Recovery Data

Debris in the DISCO vessel was recovered from five locations: (1) all cavity surfaces (Fig. 8), (2) all surfaces in the subcompartment, (3) on the cover of the subcompartment, (4) on the vessel wall, dome surface, and structures inside the containment (Fig.9), and (5) in the vertical annulus between the containment vessel wall and the subcompartment wall and on the small annular floor. The RPV-vessel (crucible) was weighted pre- and post-test. The color of the debris was gray in all tests except in test H04, where no steam was present (Fig.10). Here the debris had a brown color. Note, that Fe_3O_4 and FeO are black and Fe_2O_3 are red. A posttest sieve analysis was performed separately of the debris that was recovered from the subcompartment and the containment. A standard set of 17 sieves was used (10 mm to 40 μm) (Fig.11). Only debris particles that had diameters smaller than 10 mm were analyzed.The debris in the cavity was found on the pit floor and on top of the concrete annulus below the main cooling lines. The melt film in the vertical cavity wall was thin (~ 1 mm). Much of the debris in the subcompartment was found at the vertical wall and below, opposite of the cooling line stubs. The debris in the containment was generally collected as small particles on the walls, the top cover and on the floor. Only where melt had hit some hosepipes, melt films had formed. The particle size distribution is shown in Fig.12, separate for the particles collected in the subcompartment and the containment for test H03. In tests H01, H02, H04 and H06, much more melt was ejected directly into the containment than into the subcompartment. On the other hand, without a direct path from the pit into the containment (H03, H05) the gas and the debris has to flow first into the subcompartment and then through relatively small cross sections into the containment. Thus, most of the melt that was dispersed from the pit was trapped in the subcompartment, and very little mass reached the containment, with small particle sizes (median diameter 0.15 mm). Note, that a wire mesh covered the exits to the containment. Only few holes were burned into that mesh by melt particles. In contrast, the melt particles carried into the subcompartment have a median diameter of 3.5 mm and 4.8 mm, respectively. Fig.13 shows the cumulative particle size distribution of the total amount of debris found outside the reactor pit for all six experiments. The mean diameter of the debris particles in tests with the open cavity is

1.5 mm, while for test H03 and H05 this parameter is controlled essentially by the particles found in the subcompartment and consequently is much larger.

Fig. 8. Post test view of concrete cavity

Fig. 9. Melt particles at containment wall

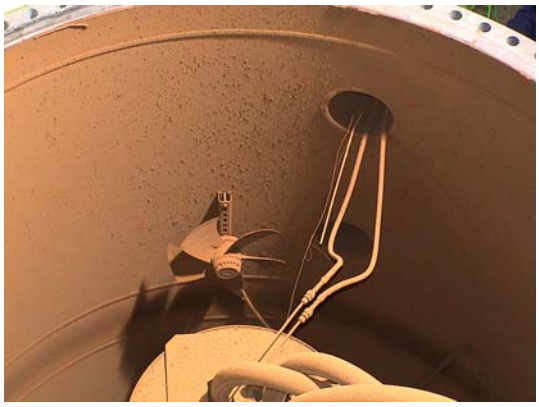

Fig. 10. Post test view into containment, H04

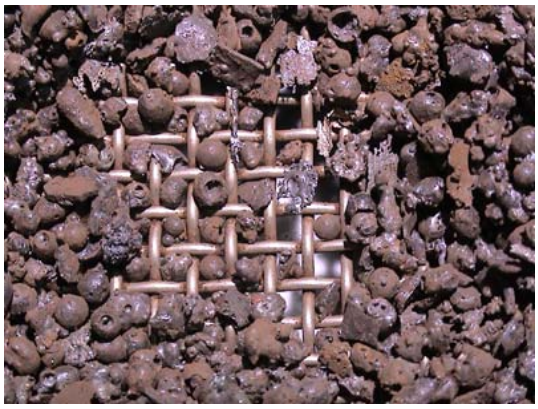

Fig. 11. Particles with diameter 2.5 > d > 1.8 mm

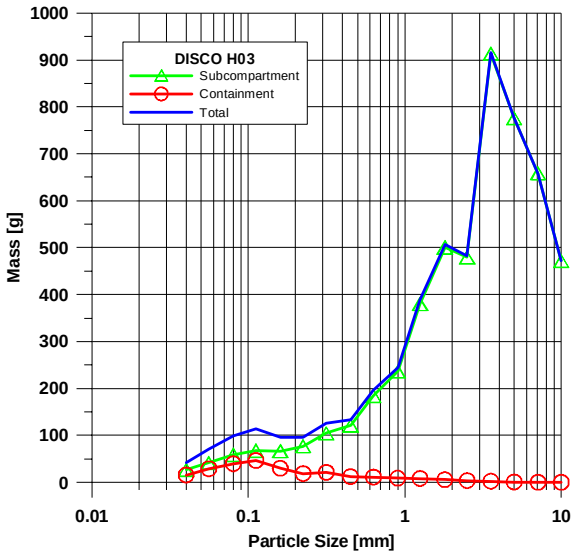

Fig. 12. Particle size distribution of debris in H03

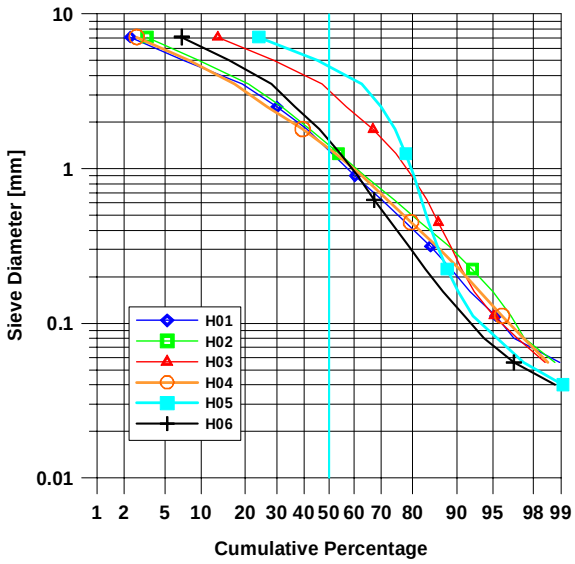

Fig. 13. Cumulative particle size distribution

4. ANALYSIS

The DISCO-H experiments are analyzed with the code AFDM (Bohl, 1992). The objective of the calculations is to develop a 2D model of the 3D experiment that describes all relevant flow paths and volumes that contribute to the DCH scenario, and to identify and quantify the physical processes relevant during melt ejection.

The DCH part of the code consists of several sections describing

1. The formation of liquid films at the walls of the cavity and the entrainment of fluid out of these films
2. Heat transfer from these films to the cavity walls and the crust formation and ablation
3. The chemical processes between the melt and the ambient mixture of steam and several noncondensible gases.
4. The valves of the experiment that are placed between the steam accumulator and the pressure vessel, and the breach opening at the bottom of the pressure vessel
5. The breach ablation and enlargement of the breach as a consequence of heat transfer from the melt to the vessel wall
6. The jet disintegration at the exit of the breach
7. The steam-melt interaction within the pressure vessel
8. The hydrogen generation in the containment due to melt steam interaction
9. The hydrogen combustion in the oxygen-rich atmosphere of the containment and the heat rejection to the containment structures

During the recalculations of the experiment, the following picture of the phenomena during melt dispersion has evolved. The flow of melt to the outside of the pressure vessel is governed by the upstream and downstream conditions. During the DISCO-cold experiment where the simulant material was water, the phenomena leading to a gas blow-through have been identified to influence the dispersion (Wilhelm, 2000). The liquid melt first leaves the breach in an almost single-phase liquid flow. At a given low liquid level in the pressure vessel, the jet becomes two-phase. This is the time of gas blow-through. The change in flow regime not only influences the mass flow through the breach but also gives way for steam entering the cavity which entrains melt from the melt films and oxidizes the metal component of the melt. The jet leaving the breach may partly disintegrate due to the shear forces acting on it. Droplets leaving the jet may have different sizes than those being formed when the jet impinges on the cavity bottom. However, due to the lack of measurements, both processes are being addressed by the same droplet generation model. Downstream of the impact area, a film of the liquid melt may be formed on the cavity bottom and the side walls. Droplets may be entrapped into the film. The rest of the droplets, especially those of a small size, may leave the cavity without contact to the cavity walls. The melt in the film exchanges heat with the colder walls. A part of the film may freeze and form a thin crust on the wall. The vapor flow may entrain droplets out of the film. These droplets are generally small enough to be levitated by the vapor flow and are thus swept out of the cavity. The reaction between the metal component of the droplets and the steam in the cavity is exothermic, and the products are oxides and hydrogen. Inside the cavity, there is not enough oxygen for hydrogen combustion. However, when hydrogen leaves the cavity, conditions are met in the reactor dome for combustion which heats up the dome atmosphere. A part of the combustion energy is directly radiated to the colder containment surfaces.

All six experiments of the present DISCO series have been recalculated. The code parameters have been kept unchanged except for first, the geometry when changing from open to closed cavity, second, the hydrogen parameters, see below, and third, the steam parameters in the reactor pressure vessel. In the experiment and the code, the steam is produced in the accumulator. After opening the valve to the pressure vessel, the steam entering the pressure vessel is heated up by the hot thermite.

The steam distribution and heat up depends on phenomena which are difficult to be modeled in the code. The code was modified several times during the recalculation of the six experiments. Therefore, different input parameters have been used. Each time, the major objective has been achieved, the good agreement between experimental and calculated pressures. Figures 14 to 19 show the pressures in the pressure vessel, the cavity, and the containment for the six experiments. In the code, droplet and bubble sizes are space and time dependent. Interfacial area convection equations have source terms that model dynamic forces, coalescence, surface forces, and more. In the cavity, the pressure rises above that of the containment because the formation of small droplets increases the surface area to the ambient gas-vapor flow and leads to a rapid heat exchange. The magnitude of this phenomenon depends on the location. Pressure peaks near the breach are usually higher. In the cases with steam-melt interaction, the exothermal heat flows to the droplets which heat up. The code model distributes this heat equally to all droplets in the cavity.

As already indicated above, the hydrogen generation is calculated in the cavity with a model that is based upon the fluid dynamics of an average melt droplet in the gas-steam atmosphere of the cavity. The chemical reaction is governed by the diffusion of steam through the gas boundary layer to the surface of the melt droplets. This gives the reaction rate in the cavity. For DISCO-H02, Fig. 20 shows the cavity inventory of steam, oxygen and hydrogen. It shows that after the steam present before breach opening has been consumed, there is a steam shortage. Only so much steam can react with the large amount of droplets as is supplied by the flow through the breach. The reaction fades out when the droplets leave the cavity. In the containment dome, there may also be hydrogen generation, but at the same time hydrogen combustion. The code has no mechanistic model for these interconnected processes. A hydrogen generation rate for the whole dome volume is an input parameter as well as the total amount of hydrogen generated. The hydrogen combustion rate is proportional to the given generation rate.

For DISCO-H02, Fig. 21 shows the total hydrogen generated as a function of time. It shows that up to 0.5 s, 0.048 kg is generated in the cavity. Between 0.6 and 1.6 s, 0.059 kg is produced in the containment. In the case of a closed cavity, the hydrogen flows first into a subcompartment. There is little oxygen there, and the droplets are directed towards the lateral surface. Therefore, there is little chance for additional hydrogen generation in the subcompartment. For DISCO-H03, Fig. 22 shows the total hydrogen of 0.042 kg which is exclusively generated in the cavity.

The hydrogen combustion rate has an influence on the pressure rise in the containment. For the maximum pressure in the containment, the heat losses play an important role. If, as expected for the open cavities, there is a standing hydrogen flame in the dome, the hot flame surface radiates a part of its heat to the containment structures. There are special codes that treat the associated phenomena in detail (Travis, 2003). The AFDM code has as an input a multiplier on the associated structure surface. The multiplier should change with the model scale. It has been kept unchanged for the present calculations.

The hydrogen generated in the experiment is relatively large compared to a prototypic case because the metal content of the thermite is higher than that of a corium containing for example 20mass% of steel. This surplus of chemical potential of the experiment makes up the loss of initial melt temperature. Extrapolating to reactor conditions must be done by comparing the effects of changes in initial melt temperature and melt composition at the same time.Table 6 collects the main hydrogen parameters, and compares hydrogen results to those of the experiment. The Experiment H04 is missing because there was neither steam nor hydrogen in the system. The table shows that for closed flow paths between the cavity and the containment there is no hydrogen generated in the containment. For H02, similarly large parts are being produced in the cavity and the containment, however for H06 with its large initial pressure, the time that steam and droplets are together in large quantities in the cavity is smaller, and the amount of hydrogen produced there is only half of that produced in the dome.

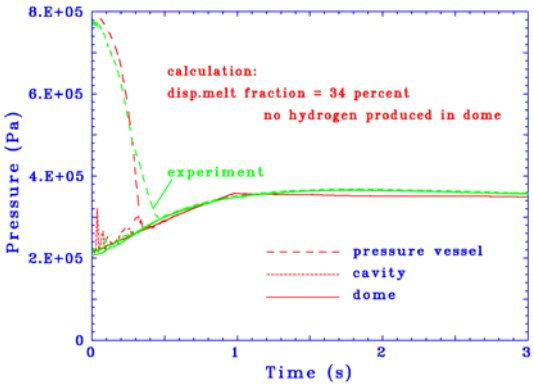

Figure 14. Pressures of DISCO-H01

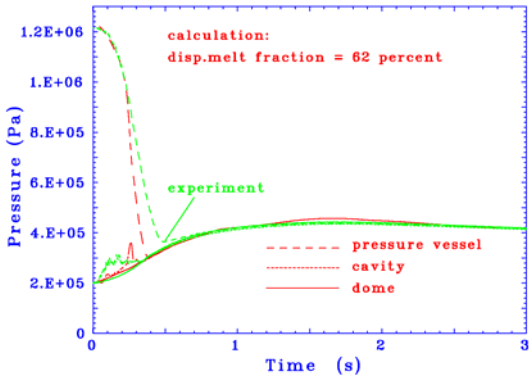

Figure 15. Pressures of DISCO-H02

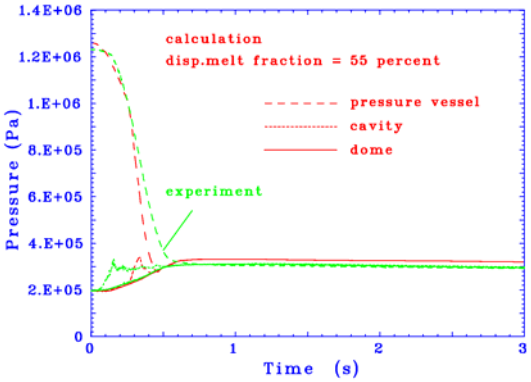

Figure 16. Pressures of DISCO-H03

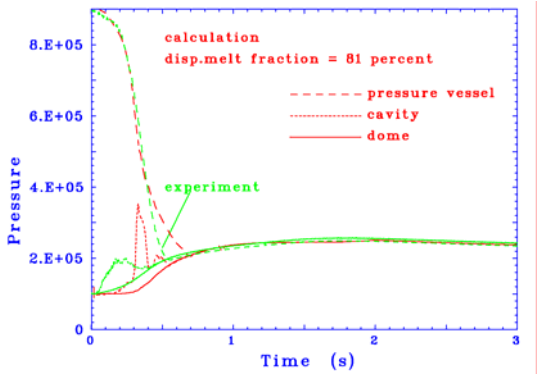

Figure 17. Pressures of DISCO-H04

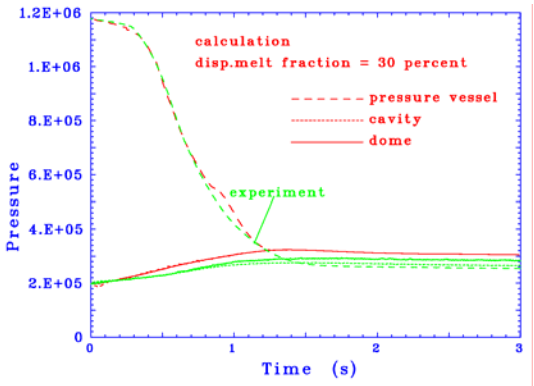

Figure 18. Pressures of DISCO-H05

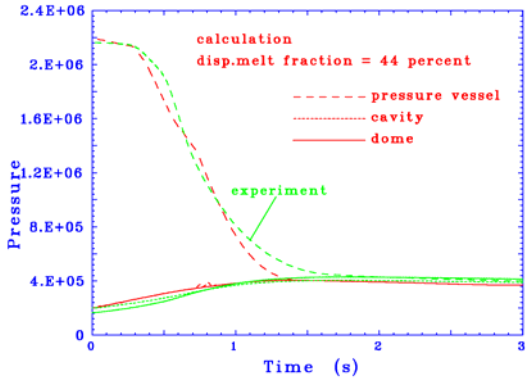

Figure 19. Pressures of DISCO-H06

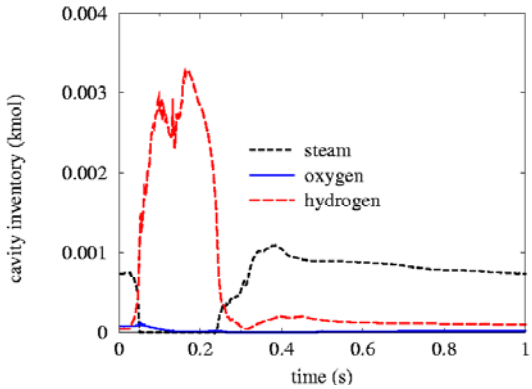

Fig. 20. Calculated cavity inventory of DISCO-H02

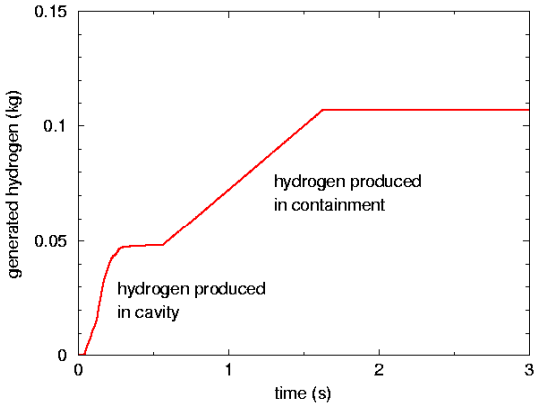

Fig. 21. Generated hydrogen of DISCO-H02

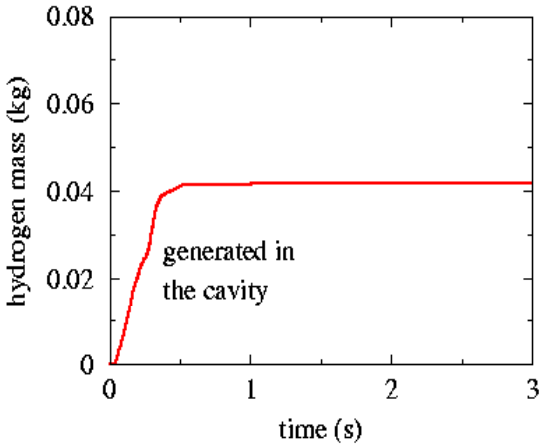

Fig. 22. Generated hydrogen of DISCO-H03

Table 7 shows integral results of the experiment and the code. For open cavities, the code does not distinguish between dispersed into the containment or into the subcompartment because subcompartment and dome share the same volume.

Table 6. Hydrogen parameters (upper section) and results (lower section)

	H01		H02		H03		H05		H06	
Flow path to containment	open		open		closed		closed		open	
	Exp.	Code	Exp.	Code	Exp.	Code	Exp.	Code	Exp.	Code
H_2combustion rate, mole/s		25		55		45		25		55
Hydrogen produced, mole		13		53		25		32		39
Hydrogen pretest, mole	--	24	26	25	27	24	29	24	35	34
H_2 prod. in cavity, mole		13		24		25		32		15
H_2 prod. in dome, mole		0		29		0		0		24
Hydrogen produced, mole	--	13	54	53	33	25	32	32	39	39
Hydrogen left, mole		8		12		25		42		19
Hydrogen burned, mole	--	24	66	66	33	24	26	14	49	54

Table 7. Additional integral results

	H01	H02	H03	H04	H05	H06
Flow path to containment	open	open	closed	open	closed	open
RPV pressure at failure, MPa	0.77	1.22	1.25	0.89	1.21	2.16
Max. exp. dome pressure increase, MPa	0.170	0.236	0.114	0.156	0.090	0.194
Max. code dome pressure increase, MPa	0.141	0.257	0.128	0.151	0.122	0.206
Exp. melt dispersed from cavity, fraction	0.36	0.61	0.46	0.75	0.38	0.49
Code melt dispersed from cavity, fraction	0.34	0.62	0.55	0.81	0.30	0.44
Exp. melt dispersed into dome, fraction	0.24	0.50	0.02	0.66	0.02	0.36
Code melt dispersed into dome, fraction	--	--	0.07	--	0.001	--

4. SUMMARY

Six experiments were performed in the DISCO-H test facility to investigate DCH phenomena in a scaled geometry of a European reactor with a tight cavity. Because the system pressure at core melt accidents will be low in German plants, the experiments were run at RPV failure pressures below 2.2 MPa. The conditions were chosen as close as possible to anticipated conditions during a severe accident. The melt was part metal part oxide, however at a lower temperature, and the atmosphere in the containment was air, steam and some hydrogen at elevated temperature and pressure. To determine the contribution of hydrogen combustion one test was performed with nitrogen and air only. All breaches were holes at the center of the bottom head, which lead to higher melt dispersal, but may be less likely than breaches at the side of the lower head. The main conclusions from the experiments are:

1. The largest melt fraction that was dispersed out of the cavity was found in the experiment without steam (74%). The reason is probably the lower back pressure in the cavity and the higher density of nitrogen versus steam and hydrogen.
2. When the reactor cavity has no direct exit to the containment, more melt remains in the reactor pit (>50%) and only 2% reaches the containment. All the rest is trapped in the subcompartment.
3. A smaller cross section of the hole leads to less dispersion (at the same failure pressure).
4. Higher failure pressure only partly compensates the smaller hole in respect to melt dispersed from the cavity.
5. The size of the debris particles ejected into the containment is small with a Sieve Mass Median Diameter (SMMD) smaller than 1.4 mm. With a closed pit it is only 0.15 mm. Larger particles are found in the subcompartment with a SMMD between 1.5 and 4.8 mm. No effect of pressure on particle size was found.
6. The maximum pressure in the containment was 0.44 MPa at 1.75 seconds after RPV failure. After 10 seconds it had decreased to 0.32 MPa. The pressure decreased although the hydrogen burned for up to 6 seconds.
7. With an open pit and hydrogen combustion the pressure rise is highest. Without a direct path into the containment less hydrogen is produced and burned. The pressure rise in the containment correlates to the amount of hydrogen burned. However, there is also a considerable pressure rise in the test without steam and hydrogen, presumably because of the efficient heat transfer from the large amount of dispersed melt into the containment.

The experiments performed with nearly prototypical conditions in a small scale showed the importance of the direct path from the reactor pit to the containment. If that path does not exist, there will be a considerable ejection into the pump and steam generator rooms, but almost nothing into the open space of the containment. On the experimental scale the pressure increase will stay moderate and well below the design pressure of most containments. This applies for failures in the lower part of the RPV bottom head, at failure pressures between 1 and 2 MPa. Without having done a hot test with lateral breaches yet, and no code calculations, we can only estimate the consequences of lateral breaches to be lower than those of more central breaches, taking the results from cold tests as reference. The comparison of two tests with and without steam, but both with hot melt, furnishes valuable data for model development concerning the effects of heat transfer, metal oxidation by air or steam and hydrogen production and combustion. All processes affect both, the melt dispersal, and the temperature and pressure load on the containment. Detailed data can be found in (Meyer,2004).

The DISCO thermite experiments are accompanied by analyses with the computer code AFDM that calculates mass, energy, momentum, and interfacial arias of thermite, steam, and noncondensible gases varying over space and time. A complete visualization of major physical processes becomes thus available. For the comparison with experimental results, the code provides pressures, melt dis-

persions, and hydrogen generation and combustion values. Above these, it is possible to distinguish where the hydrogen is generated. The calculations have shown that the results compare well with those measured. However, dispersed melt fractions are very sensitive on interactions between steam and thermite in the cavity. When extrapolating to reactor conditions, a sensitivity analysis is therefore mandatory.

ACKNOWLEDGEMENT

We are grateful to Dr. T.Blanchat, Sandia National Laboratories, for his advice and information on experimental procedures. The work of the IKET team that performed the experiments is gratefully acknowledged. This work was partially funded by the German VdEW and Siemens under the contract for the Collaboration in Research and Development for the Investigation of the Events in Severe Accidents in LWRs, and part of the work was supported by the European Commission under the contract FIKS-CT-1999-00003 (ECOSTAR, 5th EC-Framework Program).

REFERENCES

T.K. Blanchat, M.D. Allen, M.M. Pilch, R.T. Nichols, 1994, Experiments to Investigate Direct Containment Heating Phenomena with Scaled Models of the Surry Nuclear Power Plant, NUREG/CR-6152, SAND93-2519, Sandia Laboratories, Albuquerque, N.M.

T.K. Blanchat, M.M. Pilch, M.D. Allen, 1997, Experiments to Investigate Direct Containment Heating Phenomena with Scaled Models of Calvert Cliffs Nuclear Power Plant, NUREG/CR-6469, SAND96-2289, Sandia Laboratories, Albuquerque, N.M.

T. K. Blanchat, M.M. Pilch, R.Y. Lee, L. Meyer, AND M. Petit, 1999, Direct Containment Heating Experiments at Low Reactor Coolant System Pressure in the Surtsey Test Facility, NUREG/CR-5746, SAND99-1634, Sandia National Laboratories, Albuquerque, N.M.

W.R. Bohl, Wilhelm D., 1992, The Advanced Fluid Dynamics Model Program: Scope and Accomplishment, *Nuclear Technology*, **99**, pp. 309-317.

L. Meyer, M. Gargallo, 2003, Low Pressure Corium Dispersion Experiments with Simulant Fluids in a Scaled Annular Cavity, *Nuclear Technology*, **141**, pp.257-274.

L.Meyer, G.Albrecht, M.Kirstahler, M.Schwall, E.Wachter, G.Wörner, 2004, Melt Dispersion and Direct Containment Heating (DCH) Experiments in the DISCO-H Test Facility, FZKA 6988, Forschungszentrum Karlsruhe.

M.M Pilch, 1991, Adiabatic Equilibrium Models for Direct Containment Heating, presented at the 19th Water Reactor Safety Information Meeting, Washington, DC, SAND91-2407C, Sandia National Laboratories, Albuquerque, NM.

M.M. Pilch and M.D. Allen, 1996, Closure of the direct containment heating issue for Zion, *Nuclear Engineering and Design*, **164**, Issue1-3 , pp.37-60.

H. Roth-Seefried, A. Feigel, H.J. Moser, 1994, Implementation of bleed and feed procedures in Siemens PWRs", *Nuclear Engng. Design*, **148**, pp133-150.

B.R. Seghal, 2001, Accomplishments and challenges of the severe accident research, *Nuclear Engineering and Design*, **210**, pp. 79-94.

J. Travis, G. Necker, P. Royl, 2003, Recent Developments for GASFLOW-II, Proc. of the Tenth International Topical Meeting on Nuclear Reactor Thermal Hydraulics, NURETH-10, October 5-11, Seoul, Korea.

D.Wilhelm, 2000, Transient Code Models for Low Pressure Corium Dispersion, Proc. of the OECD Workshop on Ex-Vessel Debris Coolability, FZKA 6475, Forschungszentrum Karlsruhe.

D.Wilhelm, 2002, Chemical Reaction Models in a Code of the SIMMER-Family", Joint IAEA/NEA Technical Meeting on the Use of Computational Fluid Dynamic Codes for Safety Analysis of Reactor Systems, Including Containment, Pisa, Italy.

D.Wilhelm, 2003, Recalculation of corium dispersion experiments at low system pressure, NURETH-10, Seoul, Korea.